This full text paper was peer reviewed at the direction of IEEE Communications Society subject matter experts for publication in the ICC 2007 proceedings.

Sphere Decoder for a MIMO Multi-User MC-CDMA Uplink in Time-Varying Channels

Charlotte Dumard and Thomas Zemen
ftw. Forschungzentrum Telekommunikation Wien
Donau-City-Strasse 1/3, A-1220 Vienna, Austria
Email: dumard@ftw.at

***Abstract*— We focus on iterative detection for the uplink of a multi-carrier (MC) code division multiple access (CDMA) system based on orthogonal frequency division multiplexing (OFDM). The multiple-input multiple-output (MIMO) channel between each of the K users and the receiver is time-varying. At the receiver soft-symbol feedback is utilized for iterative linear minimum mean square error (LMMSE) channel estimation and multi-user detection after parallel interference cancelation.**

For multi-user detection we compare sphere decoding with an LMMSE detector. We show that a sphere decoder is more robust to channel estimation errors and less complex than an LMMSE detector while achieving better performance in terms of bit error rate versus signal to noise ratio.

I. Introduction

We consider the uplink of a multi-carrier (MC) code-division multiple access (CDMA) system based on orthogonal frequency division multiplexing (OFDM) with N subcarriers. We focus on a multiple-input multiple-output (MIMO) multi-user system. Each user $k \in \{1, \ldots, K\}$ has T transmit antennas and the base-station has R receive antennas. The receiver at the base-station performs iterative parallel interference cancelation (PIC) and multi-user detection, see [1], [2]. In the present work we replace the linear multi-user detector, used in [1], [3], with a sphere decoder [4]. Sphere decoding for MC-CDMA has been presented in [5], [6], performing detection for all users jointly. However, its complexity increases polynomially with the numbers of users. We perform sphere decoding for each user independently after parallel interference cancelation, which implies a complexity linear in the number of users and polynomial in the number of transmit antennas per user. Furthermore, this method allows parallel detection of the K users.

Our contribution: We demonstrate by means of Monte-Carlo simulations that sphere decoding after PIC is more robust to channel estimation errors than an LMMSE detector. For our sphere decoder, the cumulative distribution function (cdf) of the computational complexity per user is practically independent of the number of users or the quality of the channel state information. Furthermore, this sphere decoder has lower computational complexity than an LMMSE detector while achieving a better bit-error rate (BER) versus signal to noise ratio (SNR).

The rest of the paper is organized as follows: We present the system model in Section II and the sphere decoder in Section III. Simulation results are shown in Section IV and the derivation of the computational complexity is detailed in Section V. Conclusions are drawn in Section VI.

Notation: We denote a column vector by $\boldsymbol{a}$ and its i-th element with $a[i]$. The transpose of a matrix $\boldsymbol{A}$ is given by $\boldsymbol{A}^{\mathrm{T}}$ and its conjugate transpose by $\boldsymbol{A}^{\mathrm{H}}$. A diagonal matrix with elements $a[i]$ is written as $\mathrm{diag}(\boldsymbol{a})$ and the $Q \times Q$ identity matrix as $\boldsymbol{I}_Q$. The norm of $\boldsymbol{a}$ is denoted through $\|\boldsymbol{a}\|$.

II. System Model

In this section we describe the multi-antenna transmitter and the iterative multi-antenna receiver, relative to [2], [7], as well as the channel model. We denote the transmit antenna $t \in \{1, \ldots, T\}$ of user $k \in \{1, \ldots, K\}$ using the indexing (k, t).

A. Multi-Antenna Transmitter

Let us consider the transmitter of user $k \in \{1, \ldots, K\}$. Each transmit antenna (k, t) with $t \in \{1, \ldots, T\}$ sends a block of M OFDM symbols, including J pilot symbols allowing for channel estimation. The MT symbols are jointly coded, interleaved, mapped to a QPSK constellation and split into T blocks of length M. The $t-$th block is spread over all N subcarriers using i.i.d. spreading sequence $\boldsymbol{s}_{(k,t)} \in \mathbb{C}^N$. Thus, transmit antenna (k, t) sends the OFDM symbols $\boldsymbol{s}_{(k,t)} b_{(k,t)}[m]$ for $m \in \{0, \ldots, M-1\}$.

B. Iterative Multi-Antenna Receiver

The iterative receiver structure is shown in Fig. 1. The propagation channel from transmit antenna (k, t) to receive antenna r is characterized by the frequency response $\boldsymbol{g}_{r,(k,t)}[m] \in \mathbb{C}^N$ at time instant m with elements $g_{r,(k,t)}[m, q]$. The index q denotes the subcarrier index. The related effective spreading sequence is defined by

$$\tilde{\boldsymbol{s}}_{r,(k,t)} = \mathrm{diag}(\boldsymbol{g}_{r,(k,t)}[m]) \boldsymbol{s}_{(k,t)} \,. \tag{1}$$

In the following, we will omit the time index m unless necessary. The contribution of transmit antenna (k, t) to the signal at receive antenna r is $\tilde{\boldsymbol{s}}_{r,(k,t)} b_{(k,t)}$.

At receive antenna r, the signals from all transmit antennas add up

$$\boldsymbol{y}_r = \sum_{k=1}^{K} \sum_{t=1}^{T} \tilde{\boldsymbol{s}}_{r,(k,t)} b_{(k,t)} + \boldsymbol{n}_r \,. \tag{2}$$

1-4244-0353-7/07/$25.00 ©2007 IEEE

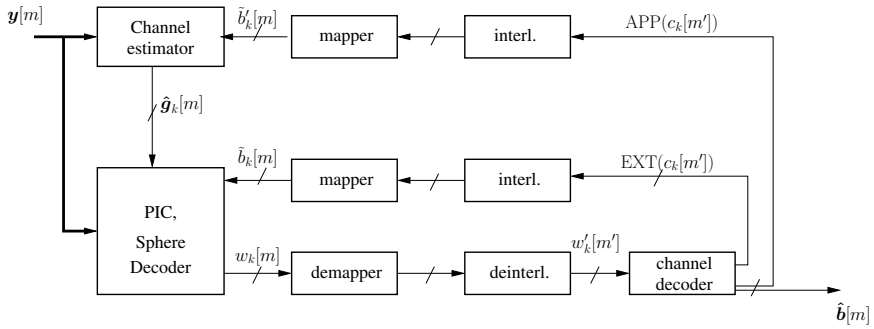

Fig. 1. The MC-CDMA receiver performs iterative time-variant channel estimation as well as sphere decoding after parallel interference cancelation (PIC).

This can be written in matrix notation as

$$\boldsymbol{y}_r = \tilde{\boldsymbol{S}}_r \boldsymbol{b} + \boldsymbol{n}_r \,, \tag{3}$$

where $\tilde{\boldsymbol{S}}_r = [\tilde{\boldsymbol{s}}_{r,(1,1)}, \ldots, \tilde{\boldsymbol{s}}_{r,(k,t)}, \ldots, \tilde{\boldsymbol{s}}_{r,(K,T)}] \in \mathbb{C}^{N \times KT}$ denotes the effective spreading matrix at antenna r and $\boldsymbol{b} = [b_{(1,1)}, \ldots, b_{(k,t)}, \ldots, b_{(K,T)}]^{\mathrm{T}} \in \mathbb{C}^{KT}$ contains all KT transmitted symbols. The noise vector $\boldsymbol{n}_r$ has zero-mean and variance $\sigma_z^2 \boldsymbol{I}_N$.

Denoting by $\boldsymbol{y} = [\boldsymbol{y}_1^{\mathrm{T}}, \ldots, \boldsymbol{y}_R^{\mathrm{T}}]^{\mathrm{T}}$ the vector containing the R received signals, we obtain

$$\boldsymbol{y} = \tilde{\boldsymbol{S}} \boldsymbol{b} + \boldsymbol{n} \,, \tag{4}$$

where $\tilde{\boldsymbol{S}} = [\tilde{\boldsymbol{S}}_1^{\mathrm{T}}, \ldots, \tilde{\boldsymbol{S}}_R^{\mathrm{T}}]^{\mathrm{T}} \in \mathbb{C}^{NR \times KT}$ contains all R effective spreading matrices. The complex Gaussian noise vector $\boldsymbol{n}$ has zero-mean and variance $\sigma_z^2 \boldsymbol{I}_{NR}$.

In (4), the contribution of user k (symbols $\boldsymbol{b}^{(k)} = [b_{(k,1)}, \ldots, b_{(k,T)}]^{\mathrm{T}}$) is defined as

$$\boldsymbol{y}^{(k)} = \hat{\boldsymbol{S}}^{(k)} \boldsymbol{b}^{(k)} + \boldsymbol{n}^{(k)} \,, \tag{5}$$

where $\hat{\boldsymbol{S}}^{(k)} \in \mathbb{C}^{NR \times T}$ contains the effective spreading sequences from all transmit antennas of user k to all receive antennas and is given by

$$\hat{\boldsymbol{S}}^{(k)} = \begin{bmatrix} \tilde{\boldsymbol{s}}_{1,(k,1)} & \cdots & \tilde{\boldsymbol{s}}_{r,(k,T)} \\ \vdots & \tilde{\boldsymbol{s}}_{r,(k,t)} & \vdots \\ \tilde{\boldsymbol{s}}_{R,(k,1)} & \cdots & \tilde{\boldsymbol{s}}_{R,(k,T)} \end{bmatrix} . \tag{6}$$

To perform detection of the user of interest k, we need to remove the contributions of all other users in (4). This is done by performing parallel interference cancelation (PIC)

$$\tilde{\boldsymbol{y}}^{(k)} = \boldsymbol{y} - \sum_{k' \neq k} \boldsymbol{y}^{(k')} \approx \boldsymbol{y} - \tilde{\boldsymbol{S}} \tilde{\boldsymbol{b}} + \hat{\boldsymbol{S}}^{(k)} \tilde{\boldsymbol{b}}^{(k)} \,. \tag{7}$$

The soft-symbol estimates $\tilde{b}_{(k,t)}[m]$ of $b_{(k,t)}[m]$ are computed from the extrinsic probabilities after detection using

$$\begin{aligned} \tilde{b}_{(k,t)}[m] = \; & \tfrac{1}{\sqrt{2}} \left(2\mathrm{EXT}(c_{(k,t)}[2m]) - 1 \right) \\ & + \mathrm{j} \tfrac{1}{\sqrt{2}} \left(2\mathrm{EXT}(c_{(k,t)}[2m+1]) - 1 \right) . \end{aligned} \tag{8}$$

Multi-user detection involves PIC (7) for user k followed by sphere decoding, which will be detailed in Section III. The $(M-J)T$ detected symbols $w_{(k,t)}[m]$ are jointly de-mapped, de-interleaved and decoded using a BCJR decoder.

C. Channel Model

We model the time-variant channel $\boldsymbol{g}_{r,(k,t)}[m]$ using the Slepian basis expansion [7]. The discrete prolate spheroidal (DPS) sequences $\{u_i[m]\}$ are defined as

$$\lambda_i u_i[m] = \sum_{l=0}^{M-1} \frac{\sin(2\pi \nu_{\mathrm{Dmax}}(l-m))}{\pi(l-m)} u_i[l] \,. \tag{9}$$

The Slepian basis function $\boldsymbol{u}_i = (u_i[m])_{m \in \{0,\ldots,M-1\}}$ are the time-limited DPS sequences corresponding to the eigenvalue λ_i, such that $\lambda_1 > \lambda_2 \ldots > \lambda_M$. The sequences $\{u_i[m]\}$ are doubly orthogonal over the infinite set $\{-\infty, \ldots, \infty\}$ and the finite set $\{0, \ldots, M-1\}$, and maximally energy concentrated on $\{0, \ldots, M-1\}$. Furthermore, they are bandlimited by

$$\nu_{\mathrm{Dmax}} = \frac{v_{\max} f_{\mathrm{C}}}{c_0} T_{\mathrm{S}} \,, \tag{10}$$

where $v_{\max}$ is the maximum (supported) velocity, T_{S} is the OFDM symbol duration, and c_0 the speed of light.

The time-variant channel $\boldsymbol{g}_{r,(k,t)}[m] \in \mathbb{C}^N$ is projected onto the subspace spanned by the first D Slepian sequences, and is approximated as

$$\boldsymbol{g}_{r,(k,t)}[m] \approx \hat{\boldsymbol{g}}_{r,(k,t)}[m] = \boldsymbol{\Gamma}_{r,(k,t)} \boldsymbol{f}[m] \,, \tag{11}$$

where $\boldsymbol{f}[m] = [u_1[m], \ldots, u_{D-1}[m]]$. In practical cases, D is in the order of 3 to 5, see [7], [8]. The coefficients in $\boldsymbol{\Gamma}_{r,(k,t)}$ are estimated using an LMMSE filter and feedback soft-symbols, as described in [1], [3].

III. Sphere Decoder

In [9] the sphere decoder for MIMO systems is presented for a single-user system and a flat-fading channel. In this section, we firstly give an introduction to ML decoding and its low-complexity implementation using sphere decoding as described in [9]. Secondly, we will use the sphere decoder for multi-user detection in the iterative MIMO multi-user MC-CDMA uplink described in the previous section.

A. Maximum Likelihood Detector

Let us consider the signal model of a MIMO single-user system in a flat-fading channel defined by

$$\boldsymbol{y} = \boldsymbol{H} \boldsymbol{b} + \boldsymbol{n} \,, \tag{12}$$

where $\boldsymbol{b} \in \mathbb{C}^T$ contains T transmit symbols, $\boldsymbol{H} \in \mathbb{C}^{R\times T}$ represents the channel, $\boldsymbol{y} \in \mathbb{C}^R$ is the received signal and $\boldsymbol{n} \in \mathbb{C}^R$ is additive complex white Gaussian noise with zero-mean and variance $\sigma_z^2 \boldsymbol{I}_R$. The system (12) has T inputs and R outputs.

The maximum likelihood (ML) detector searches for the vector $\boldsymbol{b}$ in the discrete alphabet $\mathcal{A}^T$ such that the distance $\|\boldsymbol{y} - \boldsymbol{H}\boldsymbol{b}\|^2$ is minimized,

$$\hat{\boldsymbol{b}} = \underset{\boldsymbol{b}\in\mathcal{A}^T}{\operatorname{argmin}} \{\|\boldsymbol{y} - \boldsymbol{H}\boldsymbol{b}\|^2\}\,. \tag{13}$$

The brute force implementation of a ML detector needs to search over $|\mathcal{A}|^T$ elements and its complexity increases exponentially with T. Thus, a ML detector is difficult to implement in a real-time system. However, it can be implemented more efficiently by a sphere decoder as discussed in the next section.

B. Sphere Decoder

Sphere decoders have been introduced in order to reduce the number of possible candidate vectors for the search in (13) [4], [10]. This is achieved by restraining the search to vectors $\boldsymbol{b}$ whose image through the channel (*i.e.* $\boldsymbol{H}\boldsymbol{b}$) lies within a sphere centered on $\boldsymbol{y}$ with radius ρ. This constraint is known as the sphere constraint

$$\|\boldsymbol{y} - \boldsymbol{H}\boldsymbol{b}\|^2 < \rho^2 \tag{14}$$

and allows rewriting (13) as

$$\hat{\boldsymbol{b}} = \underset{\boldsymbol{b}\in\mathcal{A}^T \,|\, \|\boldsymbol{y}-\boldsymbol{H}\boldsymbol{b}\|^2<\rho^2}{\operatorname{argmin}} \{\|\boldsymbol{y} - \boldsymbol{H}\boldsymbol{b}\|^2\}\,. \tag{15}$$

Let us consider the *thin* QR factorization of the matrix $\boldsymbol{H}$, as defined in [11]. We write $\boldsymbol{H} = \boldsymbol{Q}\boldsymbol{R}$, where $\boldsymbol{Q} \in \mathbb{C}^{R\times T}$ is a unitary matrix ($\boldsymbol{Q}^{\mathrm{H}}\boldsymbol{Q} = \boldsymbol{I}_T$) and $\boldsymbol{R} \in \mathbb{C}^{T\times T}$ is an upper triangular matrix. This factorization is unique [11].

Matrix $\boldsymbol{Q}$ being unitary, (14) becomes

$$\|\boldsymbol{z} - \boldsymbol{R}\boldsymbol{b}\|^2 < \rho^2\,, \tag{16}$$

where $\boldsymbol{z} = \boldsymbol{Q}^{\mathrm{H}}\boldsymbol{y}$. The error vector to be minimized is given by $\boldsymbol{\epsilon} = \boldsymbol{z} - \boldsymbol{R}\boldsymbol{b}$.

For $t \in \{1, \ldots, T\}$, let us define the partial vectors

$$\begin{aligned} \boldsymbol{z}^{(t)} &= [z[t], \ldots, z[R]]^{\mathrm{T}}\,, \\ \boldsymbol{b}^{(t)} &= [b[t], \ldots, b[R]]^{\mathrm{T}}\,, \\ \boldsymbol{\epsilon}^{(t)} &= [\epsilon[t], \ldots, \epsilon[R]]^{\mathrm{T}}\,, \end{aligned} \tag{17}$$

and the partial matrix

$$\boldsymbol{R}^{(t)} = \begin{bmatrix} R_{t,t} & \cdots & R_{t,T} \\ 0 & \ddots & \vdots \\ 0 & 0 & R_{T,T} \end{bmatrix}. \tag{18}$$

Matrix $\boldsymbol{R}$ being upper triangular, $\boldsymbol{\epsilon}^{(t)}$ can be written as

$$\boldsymbol{\epsilon}^{(t)} = \boldsymbol{z}^{(t)} - \boldsymbol{R}^{(t)}\boldsymbol{b}^{(t)}\,. \tag{19}$$

We denote the partial distance $d(t)$ as the norm of $\boldsymbol{\epsilon}^{(t)}$, $d(t)^2 = \|\boldsymbol{\epsilon}^{(t)}\|^2$

$$d(t)^2 = \sum_{i=t}^{T} |\epsilon[i]|^2 = d(t+1)^2 + |\epsilon[t]|^2\,, \tag{20}$$

meaning that $d(1)^2 > d(2)^2 > \ldots > d(T)^2$.

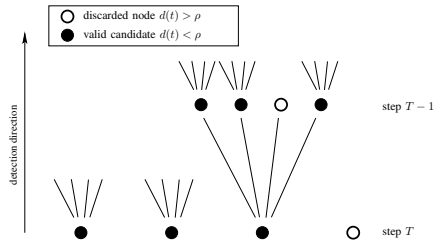

Fig. 2. Illustration of sphere decoding using tree pruning, for an alphabet with $|\mathcal{A}| = 4$ elements and T transmit antennas.

This allows for a simple iterative implementation of the sphere decoder: starting from the bottom row ($t = T$) and decreasing the index t, we compute the partial distance $d(t)$ iteratively using (20). As soon as we reach t such that $d(t)^2 > \rho^2$ (implying $d(1)^2 > \rho^2$), we discard all $\boldsymbol{b} \in \mathcal{A}^T$ having the partial $\boldsymbol{b}^{(t)} \in \mathcal{A}^{T-t+1}$.

We denote by $\mathcal{C}_t$ the set of candidates (with partial distance $d(t) \leq \rho^2$) at step t. Note that if $\rho = \infty$, the sphere decoder is an efficient implementation of an exhaustive search (*i.e.* over the whole set $\mathcal{A}^T$). In this case, we have $\mathcal{C}_t = \mathcal{A}^{T-t+1}$.

C. The Algorithm

After T steps the sphere decoding algorithm terminates. The individual steps indexed from T to 1 read as follows:

- **step T:**
  - For all $b[T] \in \mathcal{A}$, compute $d(T)^2$.
  - If $d(T)^2 \leq \rho^2$, store $b[T] \in \mathcal{C}_T$.

  $\vdots$
- **step t:**
  - For all $[b[t+1], \ldots, b[T]]^{\mathrm{T}} \in \mathcal{C}_{t+1}$ with $b[t] \in \mathcal{A}$ compute $d(t)^2$.
  - If $d(t)^2 \leq \rho^2$, store $[b[t], \ldots, b[T]]^{\mathrm{T}} \in \mathcal{C}_t$.

  $\vdots$
- **step 1:**
  - For all $[b[2], \ldots, b[T]]^{\mathrm{T}} \in \mathcal{C}_2$ with $b[1] \in \mathcal{A}$ compute $d(1)^2$.
  - If $d(1)^2 \leq \rho^2$, store $[b[1], \ldots, b[T]]^{\mathrm{T}} \in \mathcal{C}_1$.

This method can be illustrated by tree-pruning (Fig. 2) [9]. All branches leaving from a certain node are discarded when the partial distance at this node is above the threshold ρ.

After the T steps of the algorithm (note that the number of steps is equal to the number of inputs for the channel $\boldsymbol{H}$), we end up with a set of candidates $\mathcal{C}_1$ that fulfill the sphere constraint (16). If the radius ρ is chosen too small in the beginning, $\mathcal{C}_1$ might be empty (the sphere contains no symbols). On the contrary, if ρ is chosen too high, $\mathcal{C}_1$ might include all possible candidates (the sphere contains all possible symbols), thus leading back to the initial problem. It is important to define a suitable radius. We choose the radius as the distance to the zero-forcing (ZF) solution. This way we make sure $\mathcal{C}_1$ contains at least the ZF-solution given by

$$\boldsymbol{b}_{\mathrm{ZF}} = \underset{\boldsymbol{b}\in\mathcal{A}^T}{\operatorname{argmin}} \{\|\boldsymbol{R}^{-1}\boldsymbol{z} - \boldsymbol{b}\|^2\}\,. \tag{21}$$

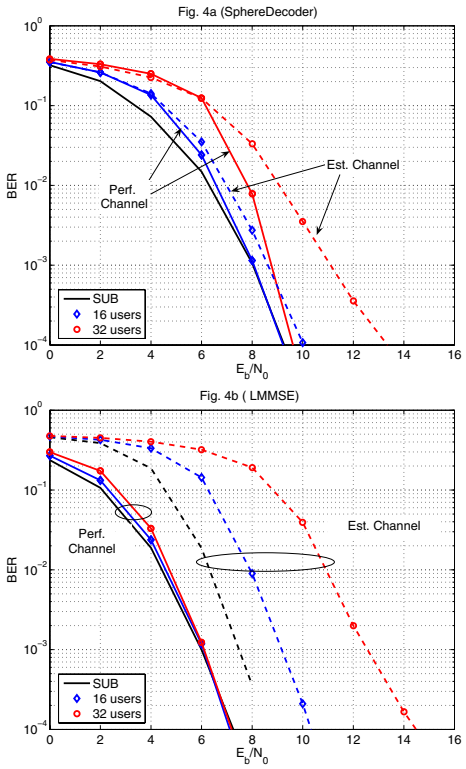

Fig. 3. BER vs SNR for $K \in \{16, 32\}$ users, $T = R = 4$ transmit and receive antennas. We compare perfect channel knowledge (full lines) and LMMSE channel estimates (dashed lines) for sphere decoding (Fig. 4a) and LMMSE detection (Fig. 4b). We also show the single user bound (SUB)

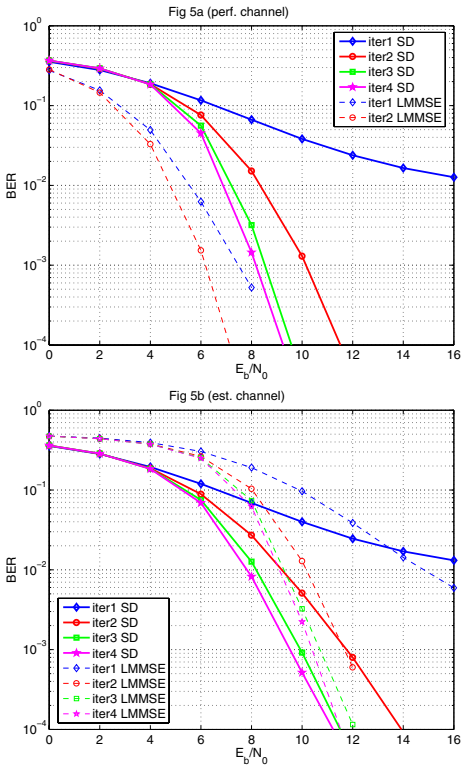

Fig. 4. BER vs SNR for $K = 24$ users, $T = R = 4$ transmit and receive antennas and perfect channel knowledge(Fig. 5a) or LMMSE channel estimates (Fig. 5b).

Finally we obtain $\rho^2 = \|\boldsymbol{z} - \boldsymbol{R}\boldsymbol{b}_{\mathrm{ZF}}\|^2$.

D. Sphere Decoding for a MIMO Multi-User MC-CDMA Uplink

By comparing (5) with (12) it becomes clear that the sphere decoder can be applied for multi-user detection in a MIMO MC-CDMA uplink as well. Matrix $\boldsymbol{H}$ (12) must be replaced by the time-varying effective spreading matrix $\hat{\boldsymbol{S}}^{(k)}$ for user k. Vector $\boldsymbol{y}$ is replaced by $\boldsymbol{y}^{(k)}$ for which we obtain an estimate $\tilde{\boldsymbol{y}}^{(k)}$ by PIC (7).

IV. Performance of the Sphere Decoder

We consider the system model described in Section II and we use the same simulation setup as in [1]. The realizations of the time-variant frequency-selective channel, sampled at the chip rate $1/T_{\mathrm{C}}$, are generated using an exponentially decaying power delay profile with root mean square delay spread $T_{\mathrm{D}} = 4T_{\mathrm{C}} = 1\mu$ for a chip rate of $1/T_{\mathrm{C}} = 3.84 \cdot 10^6\,\mathrm{s}^{-1}$. The autocorrelation for every channel tap is given by the classical Clarke spectrum [12]. The system operates at $f_C = 2\,\mathrm{GHz}$ and $K \in \{16, 24, 32\}$ users move with velocity $v = 70\mathrm{km/h}$. For these parameters the Doppler bandwidth is $B = 126$ Hz. The number of subcarriers is $N = 64$ and the OFDM symbol with cyclic prefix has length $P = G + N = 79$. The data block contains $M = 256$ OFDM symbols including $J = 60$ pilots. Each user utilizes $T = 4$ transmit antennas and the base-station has $R = 4$ receive antennas. All results are averaged over 100 independent channel realizations.

The MIMO channel taps are normalized so that

$$\mathbb{E}\left\{\sum_{r=1}^{R}\sum_{l=0}^{L-1}|h_{k,t,r}[l]|^2\right\} = 1 \tag{22}$$

in order to analyze the diversity gain of the receiver only. No antenna gain is present due to this normalization.

In Fig. 3a we show the bit error rate (BER) of the sphere decoder versus E_{b}/N_0 for $K = 16$ and $K = 32$ users. We compare the BER of the sphere decoder to the same iterative receiver using an LMMSE multi-user detector in Fig. 3b. The solid lines show the results for perfect channel knowledge, while the dashed lines show the results for LMMSE channel estimates. The BER results shown are achieved after four iterations of the receiver.

In Fig. 4 we show in more details the BER for $K = 24$ users. Here we plot all four iterations of the receiver, and we compare the behavior using sphere decoding (solid lines) or LMMSE multi-user detection (dashed lines), for perfect channel knowledge (Fig. 4a) and LMMSE channel estimates (Fig. 4b).

From these figures, we can state the following:

- with perfect knowledge of the channel, the LMMSE multi-user detector performs better than the sphere decoder;

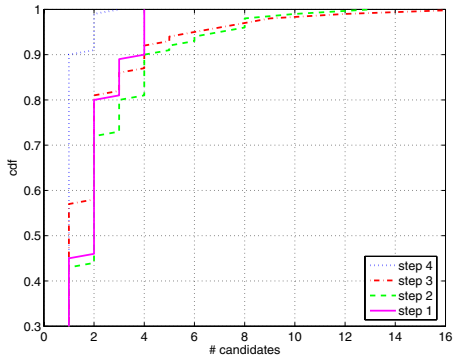

Fig. 5. Cdf of the number of candidates vectors for $K = 24$ users, $T = R = 4$ transmit and receive antennas and estimated channel. We show the $T = 4$ steps of the sphere decoding algorithm for the first receiver iteration.

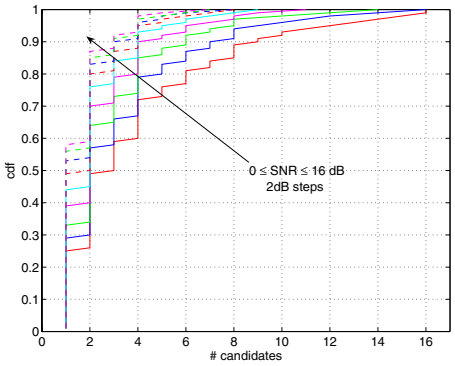

Fig. 6. Cdf of the number of candidates vectors for $K = 24$ users, $T = R = 4$ transmit and receive antennas and estimated channel for increasing SNR. We show the third step of the sphere decoder. The SNR is varying from 0dB to 16dB with 2dB-steps (the arrow shows increasing SNR).

- using channel estimates, sphere decoding outperforms LMMSE detection;
- sphere decoding is more robust to channel estimation errors (up to 3dB loss compared to 7dB using LMMSE detection, see Fig. 3).

In any practical system channel estimation is necessary, thus sphere decoding outperforms LMMSE detection in a MIMO multi-user MC-CDMA system.

V. Complexity of the Sphere Decoder

Let us here define a *flop* as a floating point operation, as given in [11]. A *flop* is an addition, substraction, multiplication, division or square root operation in the *real* domain. Thus, one complex multiplication (CM) requires 4 real multiplications and 2 additions, leading to 6 *flop*s. Similarly, one complex addition (CA) requires 2 *flop*s.

A. Complexity of the QR factorization

As a very first step we discuss the need of QR factorization. Indeed, the QR factorization usually requires high computational complexity, thus it is not straightforward that we need to perform it. We compare the computational complexity for exhaustive search, either using exhaustive search on the full matrix $\boldsymbol{H}$ or exhaustive search after a QR factorization of $\boldsymbol{H}$. The cardinality of the alphabet $\mathcal{A}$ is denoted by $\mathcal{Q} = |\mathcal{A}|$.

- For exhaustive search without QR factorization, $\boldsymbol{H}$ is a full matrix of size $NR \times T$. Thus, for all possible vectors $\boldsymbol{b} \in \mathcal{A}^T$, the computation of $\boldsymbol{Hb}$ requires $NR \times T$ CM and $NR \times (T-1)$ CA, leading to
$$\mathcal{C}_{\mathrm{ES}}^{\mathrm{noQR}} = 2Q^T NR(4T-1)\, flops\,. \tag{23}$$
- Using exhaustive search with QR factorization, we need to perform one QR factorization with complexity $T\left(4(NR)^2 - 2NRT + \frac{2T^2}{3}\right)\ flops$, see [11]. Then $\boldsymbol{R}$ has size $T \times T$ and for all possible vectors $\boldsymbol{b} \in \mathcal{A}^T$, the computation of $\boldsymbol{Rb}$ requires only $\frac{T(T+1)}{2}$ CM and $\frac{T(T-1)}{2}$ CA, leading to
$$\begin{aligned}\mathcal{C}_{\mathrm{ES}}^{\mathrm{QR}} = \;& T\left(4(NR)^2 - 2NRT + \tfrac{2T^2}{3}\right) \\ & +2T(2T+1)Q^T\, flops\,.\end{aligned} \tag{24}$$

For example, using our scenario with $R = T = 4$, $Q = 4$ for the QPSK alphabet and $N = 64$ subcarriers, we obtain:

$$\mathcal{C}_{\mathrm{ES}}^{\mathrm{noQR}} \approx 2.23 \cdot 10^6\, flops\,; \tag{25}$$

$$\mathcal{C}_{\mathrm{ES}}^{\mathrm{QR}} \approx 1.06 \cdot 10^6\, flops\,. \tag{26}$$

Performing a QR factorization first and exhaustive search later allows complexity reduction of a factor more than 2.

B. Number of Candidate Vectors in $\mathcal{C}_t$

We discuss here the computational complexity of the sphere decoder. Its complexity is not straightforward to compute, since it depends on the numbers of candidate vectors $q_t = |\mathcal{C}_t|$ retained at step $t \in \{1, \ldots, T\}$.

In Fig. 5 we show the cumulative distribution function (cdf) of the number of candidates found at each step $t \in \{1, \ldots, T\}$ of the sphere decoder algorithm, obtained from simulations. We use LMMSE channel estimate. We plot the cdf of q_t for all $T = 4$ steps. The results are averaged over 100 frames, K users and $M - J = 196$ data symbols.

For lack of space, we show simulation results only for $K = 24$ users and the first iteration of the receiver. However, more simulations allowed us to state the following conclusions:

- no sensible difference can be observed by increasing the number of users K;
- channel estimation does not affect the number of candidates compared with perfect channel knowledge;
- the cdf is similar for all receiver iterations;
- more than 90% of all cases never retain more than 5 candidates, corresponding to less than 2% of the whole candidate set (here $Q^T = 4^4 = 256$).

In Fig. 6 we show the influence of the SNR on the cdf of q_t for $1 \le t \le T$. We show results at step 3 of the sphere decoder using LMMSE channel estimates. The SNR varies in 2dB steps from 0 to 16dB, and the arrow shows increasing SNR. The results are averaged over all K users and $M - J = 196$ data symbols. As could be expected, increasing the SNR decreases the number of candidates. The same behavior occurs for the other steps of the sphere decoder.

C. Empirical cdf of the Computational Complexity

The empirical cdf of the sphere decoder computational complexity can be computed using the simulation results given in the previous subsection. We recall that $\mathcal{C}_t$ is the set of candidates after step t, $q_t \leq Q^{T-t+1}$ is the cardinality of this set and Q is the size of the alphabet $\mathcal{A}$.

The main computations at step t of the sphere decoder are

- $(T-t)$ CM and $(T-t-1)$ CA for all q_{t+1} candidates $[b_{t+1},\ldots,b_T]^{\mathrm{T}} \in \mathcal{C}_{t+1}$ from the previous step
- one CM and one CA for all $b_t \in \mathcal{A}$,

We obtain the following expression for the complexity

$$\mathcal{C}_{\mathrm{SD}} = T(8Q+2) + \sum_{t=1}^{T-1} 4q_{t+1}\left(2T-2t+1\right)\ flops\,. \quad (27)$$

Using the simulation results from Section V-B for q_t, $t \in \{1,\ldots,T\}$, we plot the empirical computational complexity cdf in Fig. 7. On the same figure, we show the complexity using an exhaustive search. Low-complexity implementation of the exhaustive search can be performed by using sphere decoding over the whole set $\mathcal{A}^T$ (with $\rho = \infty$ and $q_t = Q^{T-t+1}$), leading to an upper bound of (27)

$$\mathcal{C}_{\mathrm{SD}_\infty} = T(8Q+2) + \sum_{t=1}^{T-1} 4Q^{T-t}\left(2T-2t+1\right)\ flops\,. \quad (28)$$

We observe that for 90% of the cases, the computational complexity is lower than 30% of its upper bound.

Furthermore, we observe that the computational complexity cdf does not depend on the number of users nor if the channel is perfectly known or estimated.

D. Global Computational Complexity

The global computational complexity (*i.e.* including QR factorization and sphere decoding) can be upper bounded by (24) and (26). Using instead joint antenna LMMSE detection [13] requires the computation of a product of matrices, the inversion of a matrix of size NR as well as the computation of KT matrix-vector filters. This leads to the following complexity per user (with $K = 24$ users)

$$\begin{aligned}\mathcal{C}_{\mathrm{LMMSE}} &\approx 2T\left(\tfrac{(KT)^2}{3} + NR - KT + 8NRKT\right) \\ &\approx 1.60\cdot 10^6\, flops\,.\end{aligned} \quad (29)$$

Performing exhaustive search with a sphere decoding implementation is thus less complex than using LMMSE filtering (see (26)).

VI. Conclusions

We implemented a sphere decoder in the iterative receiver of a MIMO multi-user MC-CDMA system. We showed that a sphere decoder is more robust to channel estimation errors. Furthermore, it is less complex than an LMMSE detector while achieving better performance in terms of bit error rate versus signal to noise ratio.

Acknowledgment

The work of Charlotte Dumard and Thomas Zemen is funded by the Wiener Wissenschafts- Forschungs- und Technologiefonds (WWTF) in the ftw. project "Future Mobile Communications Systems" (Math+MIMO).

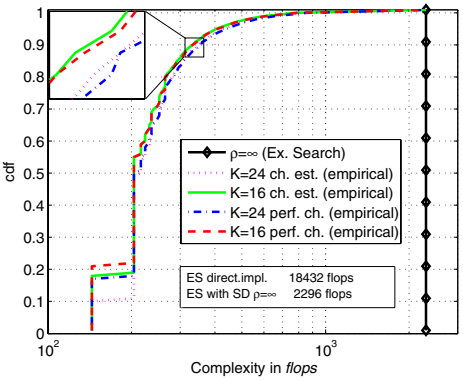

Fig. 7. Empirical cdf of the complexity in number of *flops* per symbol, per receiver iteration and per user using the sphere decoding algorithm. We also show the complexity for exhaustive search (ES) using direct implementation or sphere decoding over the infinite sphere ($\rho = \infty$). Results are for $T = R = 4$.

References

[1] T. Zemen, C. F. Mecklenbräuker, J. Wehinger, and R. R. Müller, "Iterative joint time-variant channel estimation and multi-user detection for MC-CDMA," *IEEE Trans. Wireless Commun.*, vol. 5, no. 6, pp. 1469–1478, June 2006.

[2] C. Dumard and T. Zemen, "Integration of the Krylov subspace method in an iterative multi-user detector for time-variant channels," in *Proc. IEEE International Conference on Acoustics, Speech and Signal Processing (ICASSP)*, Toulouse, France, May 2006.

[3] C. F. Mecklenbräuker, J. Wehinger, T. Zemen, H. Artés, and F. Hlawatsch, "Multiuser MIMO channel equalization," in *Smart Antennas — State-of-the-Art*, ser. EURASIP Book Series on Signal Processing and Communications, T. Kaiser, A. Bourdoux, H. Boche, J. R. Fonollosa, J. B. Andersen, and W. Utschick, Eds. New York (NY), USA: Hindawi, 2006, ch. 1.4, pp. 53–76.

[4] U. Fincke and M. Pohst, "Improved methods for calculating vectors of short length in a lattice, including a complex analysis," *Mathematics of Computation*, vol. 44, no. 169-170, pp. 463–471, April 1985.

[5] L. Brunel, "Optimum multiuser detection for MC-CDMA systems using sphere decoding," in *Proc. 12th IEEE International Symposium on Personal, Indoor and Mobile Radio Communication (PIMRC)*, 2001.

[6] ——, "Multiuser detection techniques using maximum likelihood sphere decoding in multicarrier CDMA systems," *IEEE Trans. Wireless Commun.*, vol. 3, no. 3, pp. 949–957, May 2004.

[7] T. Zemen and C. F. Mecklenbräuker, "Time-variant channel estimation using discrete prolate spheroidal sequences," *IEEE Trans. Signal Processing*, vol. 53, no. 9, pp. 3597–3607, September 2005.

[8] T. Zemen, "OFDM multi-user communication over time-variant channels," Ph.D. dissertation, Vienna University of Technology, Vienna, Austria, July 2004.

[9] A. Burg, M. Borgmann, M. Wenk, M. Zellweger, W. Fichtner, and H. Bölcskei, "VLSI implementation of MIMO detection using the sphere decoding algorithm," *IEEE J. Solid-State Circuits*, vol. 40, no. 7, pp. 1566 – 1577, July 2005.

[10] C. P. Schnorr and M. Euchner, "Lattice basis reduction: improved practical algorithms and solving subset sum problems," *Mathematical Programming*, vol. 66, no. 2, pp. 181–199, April 1994.

[11] G. H. Golub and C. F. V. Loan, *Matrix Computations*, 3rd ed. Baltimore (MD), USA: Johns Hopkins University Press, 1996.

[12] R. H. Clarke, "A statistical theory of mobile-radio reception," *The Bell System Technical Journal*, July/August 1968.

[13] C. Dumard and T. Zemen, "Krylov subspace method based low-complexity MIMO multi-user receiver for time-variant channels," in *Proc. 17th IEEE International Symposium on Personal, Indoor and Mobile Radio Communication (PIMRC)*, Helsinki, Finland, September 2006.